Available online at www.sciencedirect.com
ScienceDirect
Catalysis Today 126 (2007) 127–134
CATALYSIS TODAY
www.elsevier.com/locate/cattod

The nature of the active site in the Fe-ZSM-5/N_2O system studied by (resonant) inelastic X-ray scattering

Gerhard D. Pirngruber [a,*], Jan-Dierk Grunwaldt [a], Pijus K. Roy [a], Jeroen A. van Bokhoven [a], Olga Safonova [b], Pieter Glatzel [b]

[a] *Institute for Chemical and Bioengineering, ETH Zurich, 8093 Zurich, Switzerland*
[b] *ESRF Grenoble, France*

Available online 3 November 2006

Abstract

Resonant inelastic X-ray scattering (RIXS) was applied to investigate whether the iron–oxygen species created upon reaction of Fe-ZSM-5 with N_2O have a (partial) $3d^4$ configuration, i.e. oxidation state Fe(IV). Fe-ZSM-5 samples with low iron loading were pre-treated at high temperatures before reaction with N_2O. Then Fe K-edge XANES spectra were recorded either by selecting the fluorescence of the main $K\beta_{1,3}$ line or the satellite $K\beta'$ line in the Kβ emission spectrum. The experiments were performed in situ and imitated the experiments performed in the laboratory reactor. The absence of a pre-edge in the $K\beta'$ line spectrum proves that the configuration of the active iron–oxygen species is purely $3d^5$. The result was confirmed for several differently treated Fe-ZSM-5 catalysts. The high reactivity of Fe-ZSM-5 is therefore not due to the formation of high oxidation states of iron, but must be ascribed to the particular oxygen species that is created by the reaction of N_2O with the catalyst.
© 2006 Elsevier B.V. All rights reserved.

Keywords: X-ray absorption; X-ray emission; XANES; RIXS; Fe(IV); In situ spectroscopy

1. Introduction

Due to high stability of the benzene ring it is difficult to design appropriate catalysts that achieve a high selectivity and at the same time sufficient conversion for the direct oxidation of benzene to phenol. Current industrial routes for the production of phenol from benzene are therefore indirect, i.e. they involve the formation of other intermediates whose oxidation to phenol is easier. Some time ago it was discovered that Fe-ZSM-5, in combination with N_2O as oxidant, may be a suited catalyst for the direct oxidation of benzene, since it is almost 100% selective [1,2]. The best Fe-ZSM-5 catalysts contain very low concentrations of Fe. In addition, a special high-temperature pre-treatment is required to activate the catalyst [2–6]. The nature of the active species has been the subject of intensive research. The decisive question is how N_2O deposits its oxygen atom onto the catalyst surface and which oxygen species is so reactive and at the same time selective. Proposals for the active sites include Fe(III)–O^- radical anions [3] or Fe(IV)=O ferryl species [6], formed by the reaction

$$\mathrm{Fe(II)} + \mathrm{N_2O} \rightarrow \mathrm{N_2} + [\mathrm{Fe(III)}{-}\mathrm{O}^{\bullet -} \leftrightarrow \mathrm{Fe(IV)}{=}\mathrm{O}]. \quad (1)$$

Fe(III)–$O^{\bullet -}$ and Fe(IV)=O are mesomeric forms of the same species and can in that sense not be distinguished. It is, however, valid to ask the question whether the active species is closer to the Fe(III) radical anion or to the Fe(IV) oxo mesomer. The Fe(III)–$O^{\bullet -}$ species was proposed on the basis of Mössbauer data [3], which indicate that the oxidation state of the active species is +III. The presence of the oxygen radical anion could, however, not be confirmed by ESR spectroscopy [7]. The coupling of the spin on the oxygen radical with the spin of Fe makes the detection of the oxygen radical difficult. Until now, no direct experimental proof has been given for a Fe(IV)=O component of the active species. A Fe(IV) component should lead to a shift of the Mössbauer lines to lower energies. Mössbauer spectra of homogeneous Fe(IV) and Fe(III) complexes show that the range of typical isomer shifts of the two oxidation states are not clearly separated [8]. The interpretation of Mössbauer line shifts is therefore ambiguous.

* Corresponding author. Present address: Institut Français du Pétrole, Department of Catalysis and Separation, 69390 Vernaison, France.
Tel.: +33 4 78 02 27 33; fax: +33 4 78 02 20 66.
E-mail address: gerhard.pirngruber@ifp.fr (G.D. Pirngruber).

0920-5861/$ – see front matter © 2006 Elsevier B.V. All rights reserved.
doi:10.1016/j.cattod.2006.09.021

The same holds true for the shift of the Fe K-edge, measured in XANES spectra. Position and shape of the absorption edge do not only depend on the oxidation state, but also on covalence, band structure, geometry, etc.

We present here a different method that gives an unequivocal proof for the presence of Fe(IV) or, more precisely, of a $3d^4$ spin system, that is, resonant inelastic X-ray scattering (RIXS). A good introduction into the theory of RIXS is given, for example, in refs. [9,10]. Inelastic X-ray scattering refers to the fluorescence radiation emitted upon absorption of an X-ray photon. The fluorescence is inelastic because the emitted X-ray has a lower energy than the absorbed X-ray. The term ''resonant'' means that the absorbed X-ray photon transfers an electron from an inner shell to an unoccupied orbital close to the Fermi level instead of to the continuum. In the case of the Fe K-edge, the sample is irradiated with X-rays in the energy range corresponding to the 1s–3d transition, i.e. the so-called pre-edge peak in conventional X-ray absorption spectroscopy. The subsequent X-ray fluorescence, which results from the transfer of a 2p or 3p electron to the 1s core hole, is spectrally analyzed. For our purpose the 3p–1s (Kβ) fluorescence line is more suitable, since the exchange interaction of the 3p with the 3d orbitals is stronger than of the 2p orbitals. The Kβ emission can be resolved into a main emission line ($K\beta_{1,3}$) and a satellite (Kβ′) at lower energies. $K\beta_{1,3}$ corresponds to a parallel and Kβ′ to an antiparallel alignment of the spins in the 3d and the 3p orbital [11]. The energy of these two final states is different because of the 3d–3p exchange energy. Since the electron spin is conserved during the electron transfers $1s \rightarrow 3d$ and $3p \rightarrow 1s$, the spin orientation of the final state reflects the spin orientation of the 1s electron that was resonantly excited into the 3d shell. With high spin Fe^{3+} ($3d^5$) only a spin-down electron can be transferred and the alignment of 3d and 3p spins in the final state is parallel (see Scheme 1). Hence, no Kβ′ line is expected. With Fe^{4+} ($3d^4$) a spin-up or a spin-down electron can be transferred. Parallel and antiparallel alignment of the 3d and 3p spins is possible in the final state and resonant excitation leads to a $K\beta_{1,3}$ and a Kβ′ emission line. This difference between high spin $3d^5$ and $3d^4$ is exploited in our experiments.

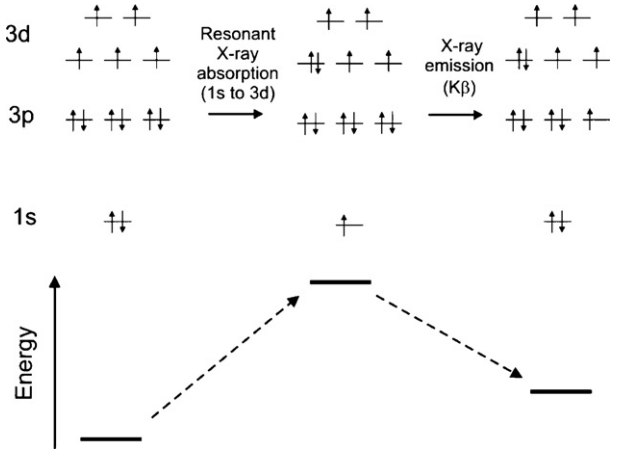

Scheme 1. Schematic representation of the RIXS process for Fe(III).

2. Experimental

2.1. Preparation of Fe-ZSM-5

NH_4-ZSM-5 was obtained by three-fold ion exchange of PZ2-40 (Zeochem, Si/Al = 24) with 1 M NH_4NO_3 solution at room temperature. A diluted aqueous solution of $FeCl_2{\cdot}4H_2O$ was used for the ion exchange, which was carried out at 353 K for 5 h in an atmosphere of N_2, to avoid oxidation of Fe^{2+} to Fe^{3+}. After filtration, washing and drying all samples were calcined in air at 773 K for 5 h. The calcined samples were subjected to a high temperature treatment in a flow of He, at 1173 or 1218 K, for 2 h (Table 1). The Fe and Al content of the samples was determined by AAS. UV–vis spectra were recorded on a Cary 400 spectrometer under ambient conditions using a Praying Mantis sample holder from Harrick. The samples are coded as Fe-ZSM-5(wt% Fe), with the suffix HT if a treatment at high temperatures was applied. Part of sample Fe-ZSM-5(0.4) was additionally steamed at 873 K for 5 h before the high temperature treatment in He. This sample is coded Fe-ZSM-5(0.4)st-HT.

2.2. Deposition of active oxygen atoms

50 mg of Fe-ZSM-5 was loaded in a laboratory quartz reactor of 4 mm inner diameter, treated at 873 K in He (purity 99.996%) for 1 h and then cooled to 523 K. A step from He to 5000 ppm N_2O in He was performed and the amount of N_2 released after the step was quantified by a mass spectrometer. It corresponds to the amount of oxygen atoms deposited on the catalyst.

2.3. Setup for operando X-ray experiments

X-ray absorption and scattering measurements were performed under conditions as close as possible to the experiments described above, i.e. using a plug flow reactor, a narrow sieve fraction of Fe-ZSM-5, and the same gas feeding device. 5–6 mg of Fe-ZSM-5 (sieve fraction 100–150 μm) was placed in a quartz capillary of 1 mm diameter and 10 μm thickness, which served as micro reactor, as described in refs. [12,13]. The capillary was placed on top of a gas blower (provided by ESRF), supplied with N_2 or Ar, which heated the sample. In order to assure a homogenous temperature distribution around the sample, a cap was placed on top of the capillary and wrapped with Al foil during the high temperature treatments and with Kapton foil during the X-ray measurements. The cap was constructed from

Table 1
Iron loading of the samples and conditions of the high temperature treatment

	wt% Fe	Fe/Al	T(HT) [K]
Fe-ZSM-5(0.1)	0.13	0.04	–
Fe-ZSM-5(0.1)-HT	0.13	0.04	1173
Fe-ZSM-5(0.4)	0.36	0.12	–
Fe-ZSM-5(0.4)-HT	0.36	0.12	1218
Fe-ZSM-5(0.4)st-HT	0.36	0.12	1218

Al to avoid excessive fluorescence radiation from metallic iron. The outlet of the capillary microreactor was connected to a mass spectrometer (Balzers Omnistar). A similar setup is described in ref. [13]. The sample was first heated to 423 K in a flow of 10 ml/min He (purity 99.9995%) to remove weakly adsorbed water. After a long dwell at 423 K (during which RIXS spectra were recorded, see below), the dehydroxylation was continued at 890 K for 1 h. After cooling to 523 K, a step from He to 5000 ppm N_2O in He was performed. The N_2 evolved after the step was quantified by the mass spectrometer signal of m/e = 28, after subtracting the contribution of N_2O, applying appropriate calibration factors [14].

2.4. (Resonant) inelastic X-ray scattering

The setup used for the (resonant) inelastic X-ray scattering experiments is shown in Fig. 1. The sample capillary was aligned to the X-ray beam at an angle of 45°. The incident X-ray energy was selected by a pair of Si crystals cut in (2 2 0) orientation. The beam was focused in a small spot (350 μm × 60 μm) on the sample. By moving the capillary along its axis it was possible to probe different positions in the sample. The scattered X-rays were monochromatized by the (5 3 1) Bragg planes of a spherical bent Si crystal and focussed on an avalanche photodiode (APD). When scanning the energy of the scattered X-rays, the APD detector and the spherical bent Si crystal were moved concertedly in order to keep the beam spot on the sample, the bent crystal and the detector on a Rowland circle. A He bag was fixed between sample, analyzer crystal and detector in order to minimize the absorption of the X-rays by air.

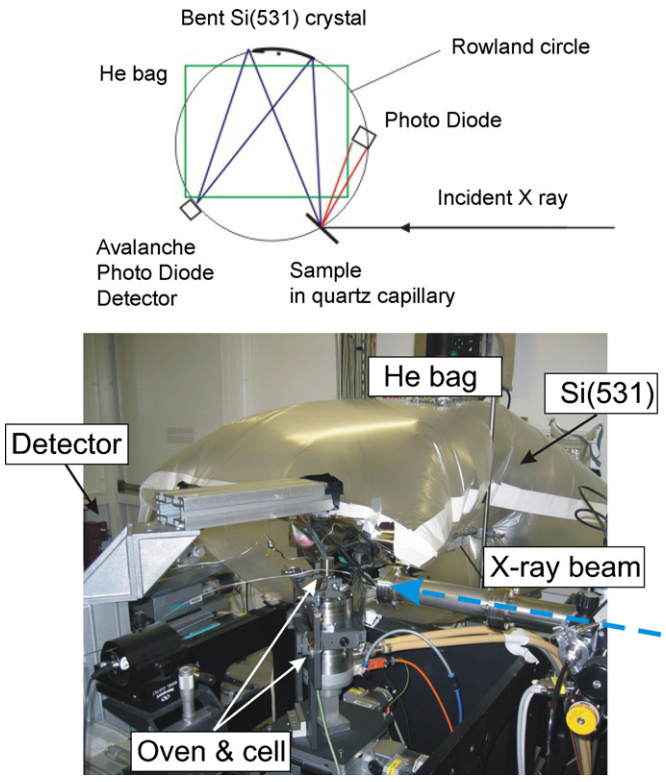

Fig. 1. Scheme and photo of the setup for the RIXS measurements.

An additional photodiode was installed next to the Si(5 3 0) crystal, to simultaneously collect conventional fluorescence X-ray absorption spectra.

In most experiments, we used a simplified procedure for the RIXS measurements. Instead of measuring the full RIXS plane, i.e. the Kβ emission spectrum for all incident energies within the 1s–3d transition, we fixed the emission energy either at the maximum of the $K\beta_{1,3}$ or the Kβ′ emission line and scanned only the incident energy. To determine the position of the main and satellite emission line, a Kβ emission spectrum (XES) was recorded first under non-resonant conditions, i.e. with an incident energy above the Fe K-edge at 7160 eV. Then the Fe K-edge was scanned, selecting either the $K\beta_{1,3}$ or the Kβ′ emission energy. The procedure was repeated several times to improve the signal to noise ratio. Each scan had a duration of 3 and 6 min, respectively, and a data point was taken each 200 ms. For the normalization purposes, additional EXAFS spectra were recorded on the $K\beta_{1,3}$ and the Kβ′ emission line. The edge jump in the XANES spectra was scaled to the normalized edge jump in the EXAFS scans.

This series of spectra (XES, XANES, EXAFS) was taken after drying a fresh sample at 423 K in a flow of He and then again after treatment with N_2O. Due to the low flux of emitted photons, the step from He to N_2O could not be followed by RIXS, and was only recorded with conventional X-ray absorption spectroscopy.

To calibrate the energy of the monochromator the following procedure was regularly applied (at least every 10 spectra): the monochromator energy was scanned from 7055 to 7060 eV while setting the Si(5 3 1) crystal to 7058.0 eV. A peak profile of the elastically scattered X-rays results from the convolution of the incoming X-ray energy bandwidth with the energy window of the analyzer crystal. The monochromator energy scale was then corrected so as to set the maximum of this peak at 7058.0 eV. The X-ray emission spectra (XES scans) were shifted to same center of gravity for comparison.

3. Results and discussion

3.1. The experimental strategy

The formation of highly active iron–oxygen species upon reaction with N_2O takes place efficiently in samples with 300–1000 ppm Fe [6,15,16], i.e. in samples with very low iron loadings. If the iron loading is increased further, the concentration of active sites seems to level off; i.e. the fraction of active sites among the totality of iron centers decreases. Since X-ray spectroscopy is an averaging technique it is important that a high fraction of the iron sites is involved in the formation of active Fe–O sites in order to avoid that the signal of the active species is submerged in the signal of the rest. The iron loading must be sufficiently low to achieve an efficient formation of the active sites, but also sufficiently high to obtain a decent signal to noise ratio in the X-ray measurements. As a compromise between the two factors we chose iron loadings between 0.1 and 0.4 wt%.

A high concentration of active iron–oxygen species is only formed if the samples are pre-treated at very high temperatures, that is ~1200 K or higher [6]. Ideally one would like to perform the pre-treatment at high temperature in situ on the beamline and record X-ray spectra during the process. Unfortunately, the gas blower did not allow us to achieve temperatures above 1150 K. Neither was it possible to record spectra at high temperatures: the Kapton foil, which covers the protecting cap on top of the capillary had to be replaced by an Al foil, which was not sufficiently X-ray transparent. We therefore chose a different strategy. The high temperature treatments were carried out our home laboratory. At the beamline the catalysts were only regenerated by dehydroxylation at ~900 K. Test experiments in our home laboratory showed that leads procedure leads to an efficient generation of active iron–oxygen sites during the subsequent reaction with N_2O (vide infra).

Last but not least the conditions of the reaction of N_2O with the iron catalyst have to be chosen. Our intention was to measure the active iron–oxygen species in a ''frozen'' state, i.e. under conditions where they do not react, in order to maximize their concentration on the catalyst surface. We therefore chose 523 K as reaction temperature. At 523 K N_2O reacts rapidly with the active iron sites, but the deposited oxygen atoms are stable on the catalyst surface and do not desorb [15,17]. The RIXS spectra were recorded at 523 K, during the reaction with N_2O. In some cases the catalyst was cooled to lower temperatures after the reaction with N_2O for recording the RIXS spectra (see Section 3.5). Our approach is therefore an ''in situ'' approach rather than an ''operando'' approach.

3.2. Characterization of the samples before and after high temperature treatment

The band maxima of the UV–vis spectra of Fe-ZSM-5(0.1) and Fe-ZSM-5(0.4) (see Fig. 2) at 44,000 and 37,000 cm^{-1} indicate that the samples contain isolated iron species [18,19] or weakly coupled dimers [20]. After high temperature treatment, the ligand to metal charge transfer (LMCT) bands are broadened and their intensity is reduced. None of the samples showed an absorption maximum below 30,000 cm^{-1}. The absence of strong absorptions in that region indicates that the high temperature treatment does not lead to an extensive clustering of the iron sites. The decrease in intensity of the LMCT bands after high temperature treatment is generally ascribed to the reduction of the iron sites to Fe(II) [21,22]. The same effect was observed after steaming of Fe-ZSM-5 samples [23].

Fig. 3 shows the X-ray emission spectra of the Fe-ZSM-5 samples recorded after dehydration at 423 K, and for comparison the emission spectrum of Fe_2O_3. The XES spectra of Fe-ZSM-5 and Fe_2O_3 are very similar. The splitting between main ($K\beta_{1,3}$ at ~7059 eV) and satellite emission peak ($K\beta'$ at ~7045 eV) is a bit smaller for Fe_2O_3. The splitting of $K\beta_{1,3}$ and $K\beta'$ is a function of the unpaired 3d electron density [24]. The smaller splitting of Fe_2O_3 can be attributed to an admixture of a $3d^6$ configuration to the $3d^5$ ground state. The emission spectra of the Fe-ZSM-5 samples do not change much after treatment at high temperature (not shown). This is surprising since the UV–vis spectra suggest that the iron sites are partially reduced after the high temperature treatment. Reduction should lead to a decrease of the $K\beta_{1,3} - K\beta'$ splitting.

The XANES spectra of Fe-ZSM-5 and Fe_2O_3, recorded on the maximum of $K\beta_{1,3}$ emission line are shown in Fig. 4. Compared to conventional XANES spectra the Kβ-detected spectra are much better resolved because of the line-sharpening effect [25]. The pre-edge of Fe_2O_3 is split into two peaks at 7112.6 and 7114.0 eV, with a shoulder at 7116 eV. The two peaks are ascribed to transitions to the t_{2g} and e_g orbitals of Fe^{3+} in octahedral coordination [26]. Both Fe-ZSM-5 samples exhibit only a single peak in the pre-edge, which tails towards lower energies. There is no clear difference between the spectra of the two Fe-ZSM-5 samples with different iron loading, apart from a feature in the edge at 7124 eV, which is more pronounced for Fe-ZSM-5(0.4). The position of the pre-edge peak (7114.3 eV) indicates that the oxidation state of the iron sites is +III. A single pre-edge peak is typical for Fe(III) in tetrahedral coordination, but also for Fe(III) with C_{4v} symmetry or similar distortion along one axis [27]. The difference

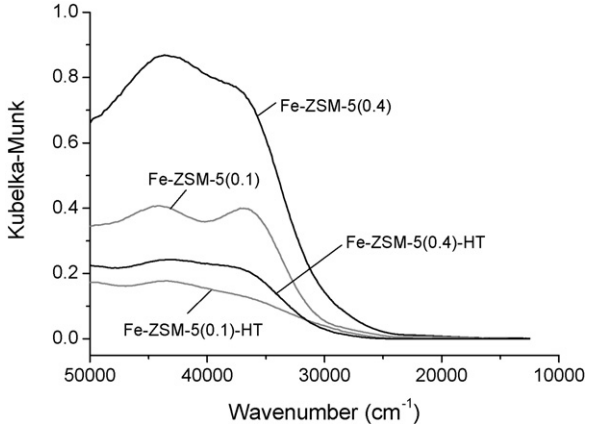

Fig. 2. UV–vis spectra of Fe-ZSM-5(0.1) and Fe-ZSM-5(0.4) before and after high temperature treatment.

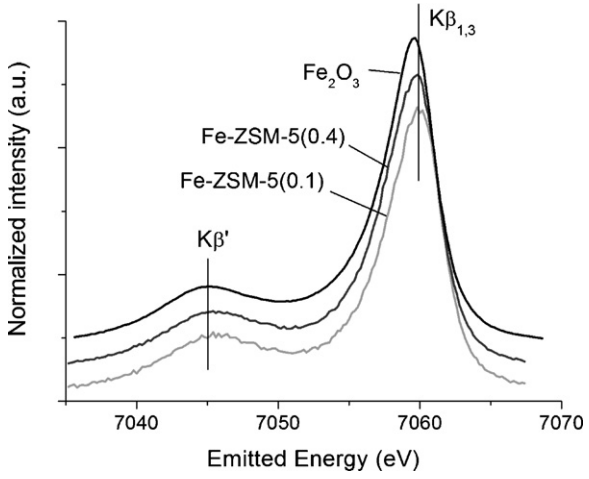

Fig. 3. X-ray emission spectra of Fe-ZSM-5(0.1) and Fe-ZSM-5(0.4), measured at 423 K in flowing He, and of Fe_2O_3.

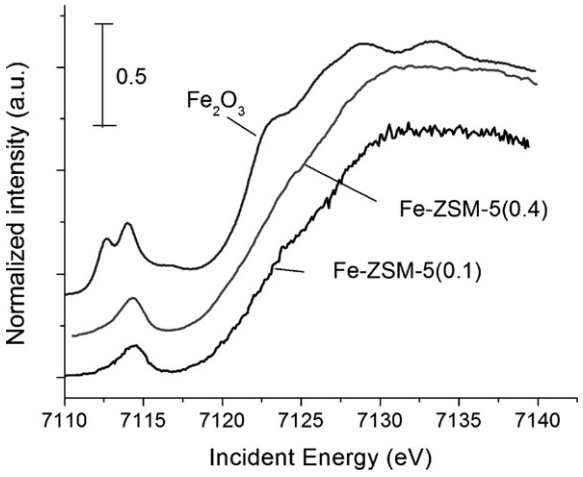

Fig. 4. Kβ$_{1,3}$-detected XANES spectra of Fe-ZSM-5(0.1) and Fe-ZSM-5(0.4), measured at 423 K in flowing He, and of Fe_2O_3.

between tetrahedral and C_{4v} (distorted) symmetry is the degree of 3d–4p orbital mixing, which leads to an increase of the pre-edge intensity. The intensity of 1s–3d dipole transitions should change to the same extent. The integrated pre-edge intensity of the Fe-ZSM-5 samples is ~0.3. For a reference compound with tetrahedral coordination ($FePO_4$) a value of 0.8 was reported [25]. This intensity ratio is within the range expected for distorted Fe(III) with C_{4v} or similar symmetry [27]. When transition metal cations are located in their preferred positions within the zeolite (according to XRD data [28]), they bind to four (or three) oxygen atoms of the framework. Additional extraframework ligands may be H_2O or hydroxyl groups [29,30], which are pointing away from the zeolite pore wall. Such an arrangement would lead to a symmetry similar to C_{4v}.

High temperature treatment had no effect on the XANES spectra (Fig. 5). This result is surprising since our UV–vis spectra as well as the results reported by others [3,31–33] point to an extensive reduction of the iron sites during the high temperature treatment, which should be reflected in a change of the edge and pre-edge features. Note, however, that in our case the high temperature treatment was not performed in situ. The samples were exposed to ambient atmosphere for a long period of time between the high temperature treatment and the synchrotron measurements, which might have led to a reoxidation of the iron sites.

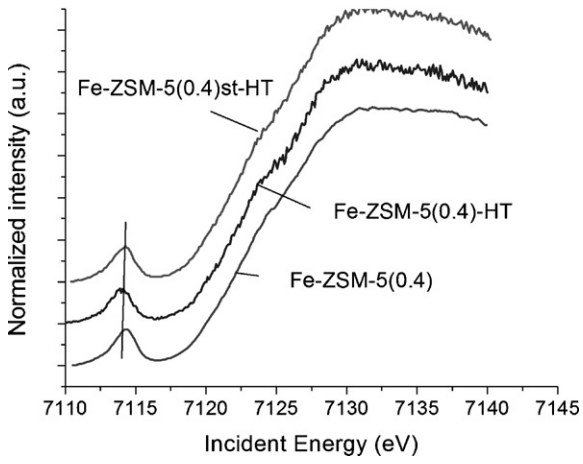

Fig. 5. Kβ$_{1,3}$-detected XANES spectra of the Fe-ZSM-5(0.4) parent sample, after high temperature treatment and after steaming and high temperature treatment. The parent sample has a better signal to noise ratio because more scans were co-added.

The UV–vis spectra were, like the XANES spectra, measured after exposure to air. The reduction in the intensity of the LMCT transitions should therefore not be attributed to the formation of Fe(II), but to a decrease of the absorption coefficient resulting from a change in the coordination geometry.

3.3. The reaction with N_2O

The goal of the synchrotron experiments was to study the reaction of N_2O with the catalyst, i.e. the deposition of active oxygen atoms on Fe-ZSM-5. To create a reference for the in situ experiments, the reaction with N_2O was first performed in a conventional laboratory reactor. Since the high temperature treatments, which generate the active sites for the reaction with N_2O, were performed ex situ, the catalysts were regenerated (dehydroxylated) by a treatment at 873 K in He before exposure to N_2O. The step from He to N_2O produced a peak of N_2, but no O_2 in the gas phase. The oxygen atom of N_2O was deposited on the catalyst surface.

$$N_2O \rightarrow N_2 + O_s \quad (2)$$

The amount of deposited oxygen atoms O_s can be calculated by integrating the N_2 peak (see Table 2). The results show that the high temperature treatment strongly increased the reactivity of the samples towards N_2O.

The deposition of oxygen atoms could be attributed to the creation of Fe(II) sites during the high temperature treatment, which are reoxidized by N_2O.

$$2Fe(II) + N_2O \rightarrow 2Fe(III) + O_s(-II) + N_2 \quad (3)$$

In that case one would expect a stoichiometry of 0.5 N_2/Fe (or less, if only a fraction of the iron sites is +II). The amount of deposited oxygen atoms is, however, much higher, close to N_2/Fe = 1 (Table 2). This stoichiometry is characteristic for the highly reactive sites that are generated by the high temperature treatment [3,6] and can be attributed to reaction (1). Our high temperature treatment, followed by in situ regeneration at somewhat lower temperature (873 K), was therefore successful

Table 2
Amount of N_2 formed in the reaction of Fe-ZSM-5 with N_2O at 523 K

	Laboratory reactor N_2/Fe	In situ synchrotron N_2/Fe
Fe-ZSM-5(0.1)	0.13	n.d.
Fe-ZSM-5(0.1)-HT	0.99	0.5
Fe-ZSM-5(0.4)	0.11	n.d.
Fe-ZSM-5(0.4)-HT	0.98	0.5
Fe-ZSM-5(0.4)st-HT	n.d.	0.5

in generating the active iron–oxygen species that we wanted to investigate by RIXS.

During the synchrotron experiments we imitated the conditions in the laboratory reactor as closely as possible. The quartz reactor of 4 mm inner diameter was replaced by a quartz capillary of 1 mm diameter. The amount of catalyst was reduced by a factor of 10 and the flow rate by a factor of 2.5. Otherwise a similar procedure was followed, i.e. pre-treatment in He at 890 K followed by reaction with N_2O at 523 K. The step from He to N_2O at 523 K was followed by XANES. The switch to N_2O resulted in a rapid shift of the Fe K-edge to higher energies (Fig. 6). After the first spectrum in N_2O, the edge did not change any further. The final XANES spectrum was almost identical to that of the parent sample, with oxidation state +III. During the regeneration (dehydroxylation) at 890 K in He the sample was partly reduced to Fe(II) and then rapidly reoxidized by N_2O. The edge shift (at half height of the edge) upon reaction with N_2O was about 0.8 eV. Full reduction of Fe(III) to Fe(II) normally leads to an edge shift of more than 3 eV [34]. Absorption edge positions do not linearly correlate with the charge of the absorbing atom, but also depend on covalence and coordination geometry [35–37]. It is therefore not possible to deduce a precise average oxidation state of the sample from the comparison of the edge shifts. Qualitatively we can, however, state that only a fraction of the iron sites was reduced to +II before the step to N_2O. The reaction with N_2O generated a peak of N_2 whose area corresponded to $N_2/Fe = 0.5 \pm 0.1$ (see Table 2). The ratio is smaller than in the laboratory reactor. The lower degree of reduction and the lower N_2/Fe ratios are attributed to the difficulty to rigorously exclude air and moisture from the sample during the in situ experiments. Compared to the concentration of Fe(II) sites, which is certainly smaller than 50%, the amount of deposited oxygen atoms is, however, large. We can therefore conclude that we obey the stoichiometry of $N_2/Fe(II) = 1$ for the reacting fraction of the iron sites. Our in situ treatment afforded the desired active iron–oxygen species, albeit not with a yield of 100%.

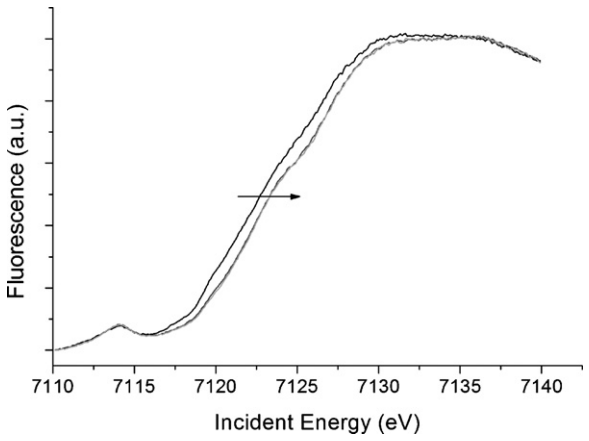

Fig. 6. XANES spectra during switch from He to N_2O at 523 K for Fe-ZSM-5(0.4)-HT. Spectra before the switch, immediately after the switch and 4 min later.

3.4. RIXS analysis of the active iron–oxygen species

If Fe(IV) species were created during the reaction with N_2O one would expect a small shift of edge and pre-edge to higher energies [38]. In our samples, only a fraction of the iron sites reacted with N_2O. The XANES spectrum results from a mixture of active and inactive spectator sites, which makes the detection of Fe(IV) via the edge shift difficult. RIXS avoids this ambiguity. If the sample contains a (partial) $3d^4$ configuration, which corresponds to oxidation state Fe(IV), it will show a pre-edge peak on the Kβ′ line spectrum. If the configuration is purely $3d^5$ (oxidation state +III) the pre-edge peak will be absent on the Kβ′ line. Fig. 7(c) shows the $K\beta_{1,3}$- and Kβ′-detected XANES spectra of Fe-ZSM-5(0.4)-HT after reaction with N_2O. The pre-edge is clearly missing in the Kβ′ line spectrum. The same result was obtained for the other HT-treated catalysts.

To make sure that the failure to detect a $3d^4$ configuration of the active iron sites was not due to an insufficient regeneration of the active sites we performed the regeneration at the maximum temperature allowed by our experimental setup, i.e. at 1130 K. After the He treatment at 1130 K, the sample was cooled to 523 K and reacted with N_2O, as usual. No pre-edge peak was detected in the Kβ′ line spectrum. Likewise, active reduction by CO at 890 K, followed by reaction with N_2O at 523 K did not lead to pre-edge peak in the Kβ′ spectrum. A reference compound $FeSrO_{2.89}$, which contains a mixture of 80% Fe(IV) and 20% Fe(III), exhibited a clear pre-edge on the satellite line [39]. The absence of the pre-edge peak in Fe-ZSM-5 proves that, in contrast to the Fe(IV) compound $FeSrO_{2.89}$, there is no electron transfer from Fe to O beyond the $3d^5$ configuration. The active iron–oxygen site should be described as a Fe(III)–$O^{\bullet -}$ species. RIXS cannot verify the nature of this oxygen species. We cannot rule out that the oxygen radical

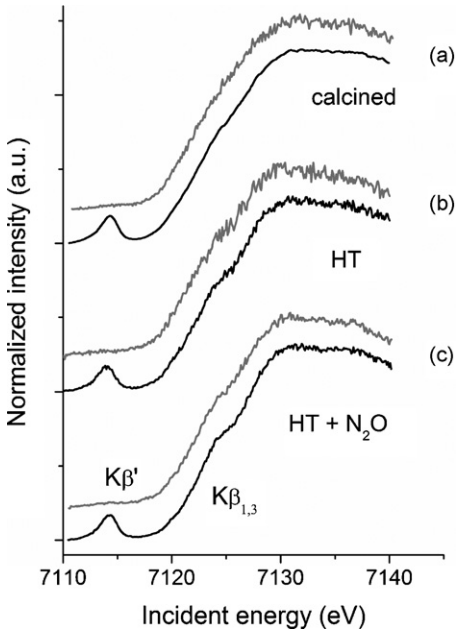

Fig. 7. $K\beta_{1,3}$- and Kβ′-detected XANES spectra of: (a) Fe-ZSM-5(0.4), (b) Fe-ZSM-5(0.4)-HT and (c) Fe-ZSM-5(0.4)-HT after reaction with N_2O at 523 K.

anion is rapidly transformed into some other surface species. It may, for example, interact with the oxygen atoms from the zeolite lattice, leading to a delocalization of the unpaired electron. We can, however, exclude that the active iron oxygen species has a significant $3d^4$ configuration, which would correspond to oxidation state Fe(IV). It is difficult to give precise detection limit of our method. A conservative estimate is that a $3d^4$ contribution of at least 10% should be clearly detectable in the Kβ′ pre-edge. The signal to noise ratio of the spectra is excellent, provided that a sufficient number of scans is accumulated, and is certainly not a limiting factor.

3.5. Beam damage

The analyzer crystal selects only a small fraction of the total X-ray fluorescence and the photon yield at the APD detector is low. RIXS therefore requires a high flux of incoming X-ray photons, especially for the samples with low iron loadings. The high photon flux may induce chemical reactions in the sample [40]. Several precautions were taken to reassure us that the X-ray beam did not destroy the active iron–oxygen species: in some experiments the reaction of Fe-ZSM-5 with N_2O was not followed by XANES, in order to avoid exposure of the sample to the beam in the presence of N_2O. The sample was cooled to 423 K, the gas flow was changed to He and only then the RIXS measurements were started. The position of the beam on the sample was changed regularly and a Kβ′ line spectrum was recorded immediately on the fresh position. None of these measures had an impact on the measured spectra. We are therefore confident that beam damage was not responsible for the failure to detect Fe(IV) species.

4. Conclusions

The present study shows the potential of resonant inelastic X-ray scattering and the application of Kβ- and Kβ′-detected X-ray absorption spectroscopy in the field of in situ characterization of heterogeneous catalysts. RIXS gives a straightforward yes/no answer to the question whether an iron sample has a $3d^4$ configuration (oxidation state +IV). The technique was applied to the active iron–oxygen species created by the reaction of Fe-ZSM-5 with N_2O. The absence of the pre-edge peak in the Fe K-edge XANES spectrum recorded on the Kβ′ emission line proves that the active species have a $3d^5$ configuration, i.e. oxidation state +III (although we cannot rule out a minor contribution of $3d^4$ which is below the detection limit of our method). This result confirms earlier Mössbauer measurements which also gave no evidence for the presence of Fe(IV) [3,41]. The high reactivity of the Fe-ZSM-5/N_2O system is therefore not due to high oxidation states of iron, but to the formation of active oxygen species bound to Fe(III).

Since RIXS operates with hard X-rays it is suitable for operando measurements of working catalysts. That is an advantage compared to techniques like Mössbauer and ESR, which are preferably carried out at low temperature. Due to the low photon yield, RIXS requires a high flux of incoming X-ray photons. It is therefore necessary to verify that beam damage does not affect the results. The low photon flux also limits the time resolution of RIXS and currently limits its application to the study of catalysts in steady state. Due to the rapid development of instrumentation, this may change in the near future.

The strategy of the present study can also be extended to further catalyst systems that have a $3d^4$ spin system, e.g. Mn(III) and Cr(II). It may also be interesting for related fields where those oxidation states are believed to play a role (e.g. enzymes, gas sensors, electrochemistry) and particularly where structure–performance relationships play a vital role.

References

[1] G.I. Panov, A.S. Kharitonov, V.I. Sobolev, Appl. Catal. A 98 (1993) 1.
[2] G.I. Panov, G.A. Sheveleva, A.S. Kharitonov, V.N. Romannikov, L.A. Vostrikova, Appl. Catal. A 82 (1992) 31.
[3] K.A. Dubkov, N.S. Ovanesyan, A.A. Shteinman, E.V. Starokon, G.I. Panov, J. Catal. 207 (2002) 341.
[4] J.F. Jia, B. Wen, W.M.H. Sachtler, J. Catal. 210 (2002) 453.
[5] E.J.M. Hensen, Q. Zhu, M. Hendrix, A.R. Overweg, P.J. Kooyman, M.V. Sychev, R.A. Van Santen, J. Catal. 221 (2004) 560.
[6] L. Kiwi-Minsker, D.A. Bulushev, A. Renken, J. Catal. 219 (2003) 273.
[7] G. Berlier, G. Spoto, S. Bordiga, G. Ricchiardi, P. Fisicaro, A. Zecchina, I. Rossetti, E. Selli, L. Forni, E. Giamello, C. Lamberti, J. Catal. 208 (2002) 64.
[8] M.P. Jensen, M. Costas, R.Y.N. Ho, J. Kaizer, A.M.I. Payeras, E. Munck, L. Que, J.U. Rohde, A. Stubna, J. Am. Chem. Soc. 127 (2005) 10512.
[9] P. Glatzel, U. Bergmann, Coord. Chem. Rev. 249 (2005) 65.
[10] F. De Groot, Chem. Rev. 101 (2001) 1779.
[11] X. Wang, F.M.F. DeGroot, S.P. Cramer, Phys. Rev. B 56 (1997) 4553.
[12] P. Kappen, J.-D. Grunwaldt, B.S. Hammershøi, L. Tröger, G. Materlik, B.S. Clausen, J. Catal. 198 (2001) 56.
[13] J.-D. Grunwaldt, M. Caravati, S. Hannemann, A. Baiker, Phys. Chem. Chem. Phys. 6 (2004) 3037.
[14] G.D. Pirngruber, P.K. Roy, Catal. Today 110 (2005) 199.
[15] I. Yuranov, D.A. Bulushev, A. Renken, L. Kiwi-Minsker, J. Catal. 227 (2004) 138.
[16] G.I. Panov, A.S. Kharitonov, V.I. Sobolev, Appl. Catal. A 98 (1993) 1.
[17] K.A. Dubkov, V.A. Sobolev, G.I. Panov, Kinet. Catal. 39 (1998) 299.
[18] J. Perez-Ramirez, J.C. Groen, A. Brückner, M.S. Kumar, U. Bentrup, M.N. Debbagh, L.A. Villaescusa, J. Catal. 232 (2005) 318.
[19] M.S. Kumar, M. Schwidder, W. Grünert, A. Brückner, J. Catal. 227 (2004) 384.
[20] G.D. Pirngruber, P.K. Roy, R. Prins, Phys. Chem. Chem. Phys. 8 (2006) 3939.
[21] J. Perez-Ramirez, M.S. Kumar, A. Brückner, J. Catal. 223 (2004) 13.
[22] M.S. Kumar, M. Schwidder, W. Grünert, U. Bentrup, A. Brückner, J. Catal. 239 (2006) 173.
[23] G.D. Pirngruber, M. Luechinger, P.K. Roy, A. Cecchetto, P. Smirniotis, J. Catal. 224 (2004) 429.
[24] U. Bergmann, M.M. Grush, C.R. Horne, P. DeMarois, J.E. Penner-Hahn, C.F. Yocum, D.W. Wright, C.E. Dube, W.H. Armstrong, G. Christou, H.J. Eppley, S.P. Cramer, J. Phys. Chem. B 102 (1998) 8350.
[25] W.M. Heijboer, P. Glatzel, K.R. Sawant, R.F. Lobo, U. Bergmann, P.A. Barrea, D.C. Koningsberger, B.M. Weckhuysen, F.M.F. de Groot, J. Phys. Chem. B 108 (2004) 10002.
[26] F.M.F. de Groot, P. Glatzel, U. Bergmann, P.A. van Aken, R.A. Barrea, S. Klemme, M. Havecker, A. Knop-Gericke, W.M. Heijboer, B.M. Weckhuysen, J. Phys. Chem. B 109 (2005) 20751.
[27] T.E. Westre, P. Kennepohl, J.G. DeWitt, B. Hedman, K.O. Hodgson, E.I. Solomon, J. Am. Chem. Soc. 119 (1997) 6297.
[28] M.C. Dalconi, G. Cruciani, A. Alberti, P. Ciambelli, Catal. Today 110 (2005) 345.

[29] B.R. Wood, J.A. Reimer, A.T. Bell, M.T. Janicke, K.C. Ott, J. Catal. 225 (2004) 300.
[30] G.D. Pirngruber, J.A.Z. Pieterse, J. Catal. 237 (2006) 237.
[31] T.V. Voskoboinikov, H.Y. Chen, W.M.H. Sachtler, Appl. Catal. B 19 (1998) 279.
[32] E. Hensen, Q. Zhu, P.-H. Liu, K.-J. Chao, R. Van Santen, J. Catal. 226 (2004) 466.
[33] L. Capek, V. Kreibich, J. Dedecek, T. Grygar, B. Wichterlova, Z. Sobalik, J.A. Martens, R. Brosius, V. Tokarova, Microporous Mesoporous Mater. 80 (2005) 279.
[34] G.D. Pirngruber, P.K. Roy, N. Weiher, J. Phys. Chem. B 108 (2004) 13746.
[35] P. Mahto, A.R. Chetal, Phys. B 158 (1989) 415.
[36] M. Kasrai, M.E. Fleet, G.M. Bancroft, K.H. Tan, J.M. Chen, Phys. Rev. B 43 (1991) 1763.
[37] A.H. De Vries, L. Hozoi, R. Broer, Int. J. Quantum Chem. 91 (2003) 57.
[38] F. Haass, T. Buhrmester, M. Martin, Solid State Ionics 141 (2001) 289.
[39] G.D. Pirngruber, J.-D. Grunwaldt, J.A. Van Bokhoven, A. Kalytta, A. Reller, O.V. Safonova, P. Glatzel, J. Phys. Chem. B 110 (2006) 18104.
[40] J.G. Mesu, A.M.J. van der Eerden, F.M.F. de Groot, B.M. Weckhuysen, J. Phys. Chem. B 109 (2005) 4042.
[41] A.R. Overweg, M.W.J. Craje, A.M. van der Kraan, I. Arends, A. Ribera, R.A. Sheldon, J. Catal. 223 (2004) 262.